Supporting Information

Peptides as Versatile Platforms for Quantum Computing

Lorena E. Rosaleny,[†] Salvador Cardona-Serra,[†] Luis Escalera-Moreno,[†] José J. Baldoví,[‡] Violetta Gołębiewska,[†] Karolina Wlazło,[†] Patricia Casino[¶], Helena Prima-García,[*,†] Alejandro Gaita-Ariño[*,†] and Eugenio Coronado[†]

† *Instituto de Ciencia Molecular, Universitat de València, Catedrático José Beltrán 2, 46980 Paterna, Spain*

‡ *Max Planck Institute for the Structure and Dynamics of Matter, Luruper Chaussee 149, D-22761 Hamburg, Germany*

¶ *Dept. de Bioquímica y Biología Molecular, ERI BioTecMed, Universitat de València, Dr. Moliner 50, 46100 Burjassot, Spain*

E-mail: helena.prima@uv.es, alejandro.gaita@uv.es

List of contents

S1 Determination of folding patterns by means of the program SHAPE

One of the first designed Lanthanide Binding Tag peptides (termed LBT in this article)[1] has the aminoacid sequence (one-letter code) shown in Table S1. The Table shows several peptides able to bind lanthanides, that have highly conserved sequences, especially in three different tracts that are enriched in acidic aminoacids (aspartates and glutamines).

Table S1. *Previously reported Lanthanide Binding Tags X-ray resolved crystal structures (except for2LR2 which was determined by NMR). # of independent Ln-binding sites > 1 is due to either duplication of peptide sequences, crystallographic inequivalence or both. Green denotes conserved aminoacidos in all proteins, bold denotes coordinating residues. Note that dozen of other variations of the same sequence have been characterized as selectively binding to lanthanide ions,*[1] *but have not been crystallized.*

protein	Ln	# indep. sites	LBT aminoacid sequence	resolution (Å)	PDB ID[ref]
LBT	Tb	2	YI**D**T**N**N**D**G**W**Y**E**GD**E**LLA	2.0	1TJB[2]
dLBT-Ubiquitin	Tb	2	GPGYI**D**T**N**N**D**G**W**I**E**GD**E**L- -YI**D**T**N**N**D**G**W**I**E**GD**E**LLA	2.6	2OJR[3]
Interleukin-1β-(S1-LBT)	Tb	1	GYI**D**T**N**N**D**G**W**I**E**GD**E**LY	2.1	3LTQ[4]
Interleukin-1β-(L3-LBT)	none	1	GYI**D**T**N**N**D**G**W**I**E**GD**E**LY	1.7	3POK[4]
xq-dSE3-ubiquitin	Gd	4	YI**D**T**D**N**D**G**S**I**D**GD**E**L- -YI**D**T**D**N**D**G**S**I**D**GD**E**LLA	2.4	3VDZ[5]
Z-L2LBT	none	1	SYI**D**T**N**N**D**GAY**E**GD**E**LSG	n.a.	2LR2[6]

SHAPE software quantifies the deviation of chemical 3D structures from either ideal geometrical structures or selected structures from the user.[7] In our case, we used it to compare the shape of LBT-containing peptides previously described in the literature with each other (see Table S1). SHAPE software determines a continuous shape parameter (SP), which is mathematically defined in a way that is independent of the size of the system. By definition, the resulting value of SP is zero when the real coordinates of the metal site (problem structure, P) show exactly the desired ideal shape, and increases with the degree of distortion of the structure. Values below 0.1 represent chemically insignificant distortions in the structure. Values larger than 3 mean important distortions, with the highest values commonly encountered being in the order of 40.

The main object for comparison were the α-carbons forming the backbone of each of the LBT-containing peptides, namely LBT peptide (molecule A and B, PDB id 1TJB), dLBT-ubiquitin (molecule A and B, PDB id 2OJR), Interleukin-1β-(S1-LBT) (PDB id 3LTQ), xq-dSE3-ubiquitin (molecule A.1, A.2, B.1 and B.2, PDB id 3VDZ) and Z-L2LBT (PDB id 2LR2). The coordinates for all of the proteins were extracted from the PDB files downloaded from the RCSB Protein Data Bank website (https://www.rcsb.org/pdb/).

It is observed that the aminoacidic sequence is highly similar from the first fifteen α-carbon atoms belonging to the LBT motif in all of the examined proteins, and it is much more variable in the sixteenth and seventeenth α-carbon atoms (table S1.1). Additionally, not all of the LBT motifs in the molecules contain seventeen α-carbons. For this reason two different sets of calculations were carried out. Regarding the first set, only fifteen α-carbons were taken into account (table S1.2), whereas the second one included seventeen α-carbons when possible (table S1.3).

Table S1.1. *Aminoacid sequence of the LBT motifs found in different chimeric polypeptides. For double LBT motifs the notation used the chain name in the PDB files (A or B) and a number to denote if the unit was first or second in the sequence.*

	Cα position in motif																
LBT motif (PDB ID)	1CA	2CA	3CA	4CA	5CA	6CA	7CA	8CA	9CA	10CA	11CA	12CA	13CA	14CA	15CA	16CA	17CA
1TJB chainA&B	TYR	ILE	ASP	THR	ASN	ASN	ASP	GLY	TRP	TYR	GLU	GLY	ASP	GLU	LEU	LEU	ALA
2OJR chainA.1	TYR	ILE	ASP	THR	ASN	ASN	ASP	GLY	TRP	ILE	GLU	GLY	ASP	GLU	LEU	-	-
2OJR chainA.2	TYR	ILE	ASP	THR	ASN	ASN	ASP	GLY	TRP	ILE	GLU	GLY	ASP	GLU	LEU	LEU	ALA
3LTQ	TYR	ILE	ASP	THR	ASN	ASN	ASP	GLY	TRP	ILE	GLU	GLY	ASP	GLU	LEU	TYR	ASP
3VDZ chainA.1&B.1	TYR	ILE	ASP	THR	ASP	ASN	ASP	GLY	SER	ASP	GLY	ASP	GLU	LEU	-	-	-
3VDZ chainA.2&B.2	TYR	ILE	ASP	THR	ASP	ASN	ASP	GLY	SER	ILE	ASP	GLY	ASP	GLU	LEU	LEU	ALA
2LR2	TYR	ILE	ASP	THR	ASN	ASN	ASP	GLY	ALA	TYR	GLU	GLY	ASP	GLU	LEU	SER	GLY

Table S1.2. *SHAPE results calculated using 15 α-carbons from the LBT motifs.*

	1TJB chainA	1TJB chainB	2OJR chainA.1	2OJR chainA.2	3LTQ	3VDZ chainA.1	3VDZ chainA.2	3VDZ chainB.1	3VDZ chainB.2	2LR2
1TJB chainA	0.000	0.147	3.174	2.312	3.113	4.092	2.135	4.243	2.116	0.260
1TJB chainB	0.147	0.000	2.553	1.829	2.409	3.665	1.787	3.715	1.783	0.206
2OJR chainA.1	3.174	2.553	0.000	1.589	0.302	0.737	2.162	0.685	2.169	3.161
2OJR chainA.2	2.312	1.829	1.589	0.000	1.481	2.258	0.551	2.114	0.591	1.998
3LTQ	3.113	2.409	0.302	1.481	0.000	1.040	1.927	0.909	1.919	3.171
3VDZ chainA.1	4.092	3.665	0.737	2.258	1.040	0.000	3.047	0.243	3.007	4.276
3VDZ chainA.2	2.135	1.787	2.162	0.551	1.927	3.047	0.000	2.849	0.013	1.897
3VDZ chainB.1	4.243	3.715	0.685	2.114	0.909	0.243	2.849	0.000	2.830	4.329
3VDZ chainB.2	2.116	1.783	2.169	0.591	1.919	3.007	0.013	2.830	0.000	1.903
2LR2	0.260	0.206	3.161	1.998	3.171	4.276	1.897	4.329	1.903	0.000

Table S1.3. *SHAPE results calculated using 17 α-carbons from the LBT motifs.*

	1TJB chainA	1TJB chainB	2OJR chainA.2	3LTQ	3VDZ chainA.2	3VDZ chainB.2	2LR2
1TJB chainA	0.000	0.409	9.343	6.180	8.095	8.321	2.839
1TJB chainB	0.409	0.000	7.530	3.956	6.801	7.023	1.477
2OJR chainA.2	9.343	7.530	0.000	7.595	0.648	0.681	5.749
3LTQ	6.180	3.956	7.595	0.000	8.342	8.540	3.570
3VDZ chainA.2	8.095	6.801	0.648	8.342	0.000	0.014	5.753
3VDZ chainB.2	8.321	7.023	0.681	8.540	0.014	0.000	5.964
2LR2	2.839	1.477	5.749	3.570	5.753	5.964	0.000

Table S1.4. *SHAPE results calculated using oxygen atoms from the LBT motifs coordination environment.*

	1TJB chainA	1TJB chainB	2OJR 15CA	2OJR 17CA	3LTQ
1TJB chainA	0.000	0.668	1.962	4.229	0.920
1TJB chainB	0.668	0.000	1.608	3.622	0.367
2OJR 15CA	1.962	1.608	0.000	1.521	1.633
2OJR 17CA	4.229	3.622	1.521	0.000	3.442
3LTQ	0.920	0.367	1.633	3.442	0.000

The oxygen atoms forming the coordination environment for each of the LBT motifs were used for SHAPE calculations presented in Table S1.4.

In sum, the analyses of the information of the tables above is the following:

-for the 15-long peptide fragment (Table S1.2), the foldings are distorted compared with each other, but remarkably similar, considering the great difference between the aminoacid sequences, for example in the case of 1TJB vs 3VDZ:

-for the 17-long peptide fragment (Table S1.3), the folding is markedly more different, signaling that the last two aminoacids do not fold reproducibly: the maximum SP parameters double compared with the previous table: from slightly above 4 to slightly above 8

-for the 8 oxygen coordination environment (Table S1.4), the shapes are distorted but again they are remarkably similar, considering the relative freedom enjoyed by the side groups (again, the maximum SP parameters are slightly above 4); here note that 3VDZ was designed for an efficient interchange of water molecules directly coordinated to the Gd, and as a consequence its coordination environment is severely distorted (although, as seen in the tables above, the folding remains essentially the same), so we did not consider it for the comparison.

Analysing Table S1.4, it is evident that there are relatively large calculated distortions between the oxygen coordination spheres of 2OJR (both 15CA and 17CA) and 3LTQ, something striking since they share the aminoacid sequence (primary structure) of the region that actually binds to the lanthanide ion, i.e. YIDTNNDGWIEGDEL. Compared with regular distortions between crystallographically inequivalent copies of identical coordination complexes, these SP parameters are rather high, which could mean that the coordination environments are difficult to reproduce. However, here it is crucial to put these SHAPE parameters in perspective, and for that one needs to note that peptide crystallography involves an uncertainty in the atomic positions that is higher than usual in coordination chemistry. For this purposes we can take as a measure the Diffraction Precision Index (DPI) as presented by Gurusaran and coworkers.[7]We employed the data analysis software accessible at the server http://cluster.physics.iisc.ernet.in/dpi/ and, as seen in Table S1.5, found that the DPI values of the peptides under study in this section range from about 0.1 to almost 0.4 Å, which means the SP parameters we calculate are in this case strongly affected by crystallographic noise. Thus, these numbers should be understood as an upper limit to the real structural difference between the peptidic foldings, in the case of Tables S1.2 and S1.3, or between the coordination environments, in the case of Table S1.4. Further studies would be needed to more accurately quantify the maximum possible distortion between the coordination spheres of two lanthanide binding tags with the same primary sequence.

Table S1.5. *Resolution and DPI regarding the protein structures studied.*

PDB ID	Resolution (Å)	Diffraction Precision Index DPI (Å)
1TJB	2.0	0.196
2OJR	2.6	0.329
3LTQ	2.1	0.097
3POK	1.7	0.077
3VDZ	2.4	0.392

Additionally, a study of the geometry of octa-coordinated Tb^{3+} in the LBT peptide (1TJB) context was performed comparing the position of coordination oxygens to vertices in reference polyhedra predefined in the SHAPE package. The results (see Table S1.6) suggested that the LBT coordination environment does not adopt an ideal geometry, but is closely related to a square antiprism (SHAPE parameter approx. 3.6), a triangular dodecahedron (approx. 3.3) or a biaugmented trigonal prism (approx. 3.4). Note however, that these descriptions are limited in precision for the above stated reasons of crystallographic uncertainty.

Table S1.6. *Geometry study of octa-coordinated lanthanide ions in an LBT unit (1TJB). SP parameters are shown. Comparisons were made with all 13 ideal geometries included as reference polyhedra for octa-coordinated metals in the SHAPE software.*

Symmetry	Geometry	1TJB chainA	1TJB chainB
D_{8h}	Octagon	30.016	30.640
C_{7v}	Heptagonal pyramid	22.975	22.496
D_{6h}	Hexagonal bipyramid	14.981	15.752
O_h	Cube	10.736	11.304
D_{4d}	Square antiprism	3.645	2.622
D_{2d}	Triangular dodecahedron	3.627	3.021
D_{2d}	Johnson - Gyrobifastigium (J26)	12.709	13.832
D_{3h}	Johnson - Elongated triangular bipyramid (J14)	26.491	27.036
C_{2v}	Johnson - Biaugmented trigonal prism (J50)	4.538	4.176
C_{2v}	Biaugmented trigonal prism	3.842	3.081
D_{2d}	Snub diphenoid (J84)	5.341	5.628
T_d	Triakis tetrahedron	11.282	12.122
D_{3h}	Elongated trigonal bipyramid	21.773	23.001

S2 Continous Wave (CW) EPR spectroscopy and pulsed EPR determination of relaxation times

EPR measurements were performed in buffer containing 10 mM HEPES at pH 7.0, 100 mM NaCl, 5 mM β-mercaptoethanol and 20 % glycerol (for cryoprotection). Thorough degassing was performed on all solutions previously to the EPR measurements, with a freeze-pump-thaw procedure as described in a work from Hirsh and Brudvig.[9] This is necessary since the presence of paramagnetic O_2 traces significantly alters pulsed EPR results in this kind of frozen samples.

The solutions measured by EPR spectroscopy contained varying concentrations of LBT peptide (from 72 μM to 144 μM) which were in excess respect to the complexing lanthanide ion.

Both continuous-wave and pulsed EPR data were recorded on an ELEXSYS E580 EPR spectrometer (Bruker) equipped with a Pulsed X-band (9.3 GHz cavity and resonators) operating in the range 4 -300 K. The external magnetic field B_0 can be applied in a range 0-2 T. The pulsed X-Band is equipped with a TWT (travelling wave tube) amplifier, and is able to perform pulses between 0.7 ns and 15 μs long.

The pulse sequences for the echo-induced spectra and for the experiments determining T_m and T_1 were based on $\tau_{\pi/2}$=12 ns, τ_{π}=24 ns pulses with a fixed interpulse delay time of τ = 200 ns. Rabi oscillations were acquired by long microwave field pulses of duration t and subsequently recorded by spin echo. The τ pulse and the π/2- π Hahn spin-echo sequence were recorded varying the attenuation power and subsequently the oscillating magnetic field B_1. The external static magnetic field B_0 was 3480 G.

(a)

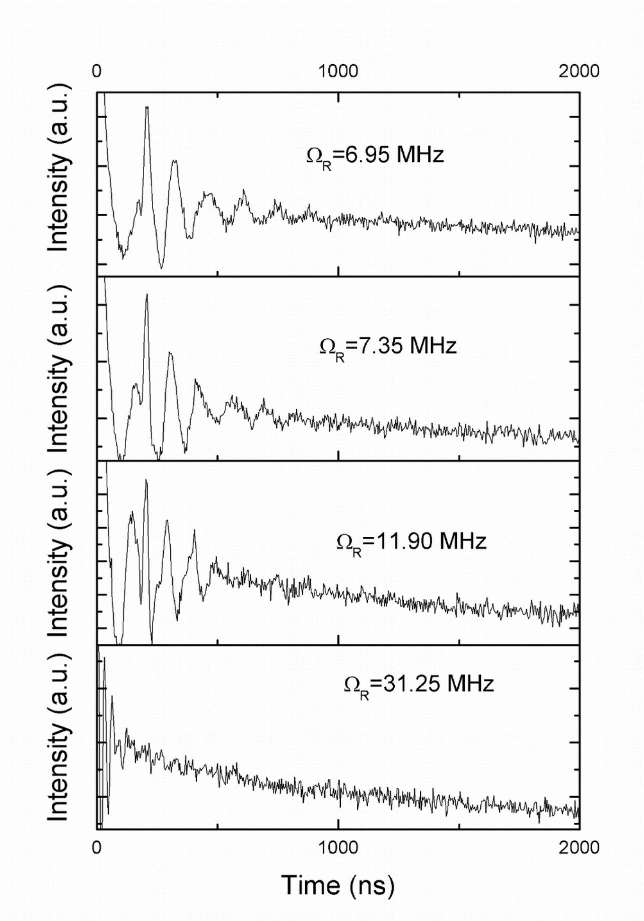

(b)

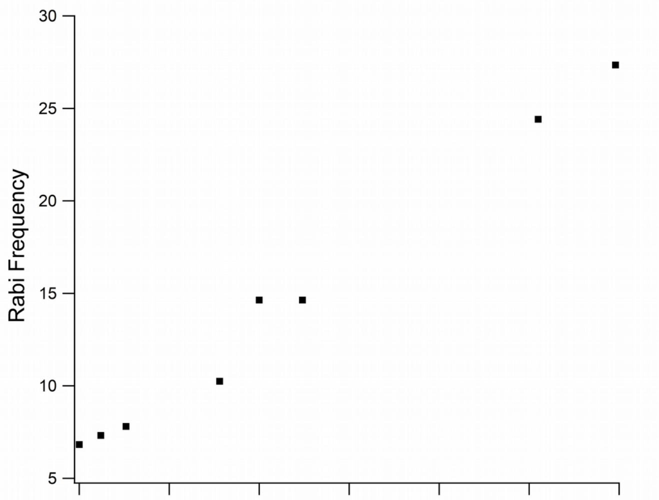

Figure S2.1. *(a) Measured $M_z(t)$ showing the result of nutation experiments at microwave powers that are above or below values where the Rabi frequency matches the Larmor frequency of the proton (Hartmann-Hahn condition) for the sample* ***GdLBT*** *at 4 K and at B_0 = 3480 G. (b) Rabi frequencies as a function of the oscillating magnetic fiekd B_1 for* ***GdLBT****. B_1 values are calculated relative to the value of B_1 at the maximum attenuation of 19 dB,* $B_1=\sqrt{10^{-0.1A}/10^{-1.9}}$ *, where A is the attenuation in dB. The off-linear points correspond to the Hartman-Hahn condition.*

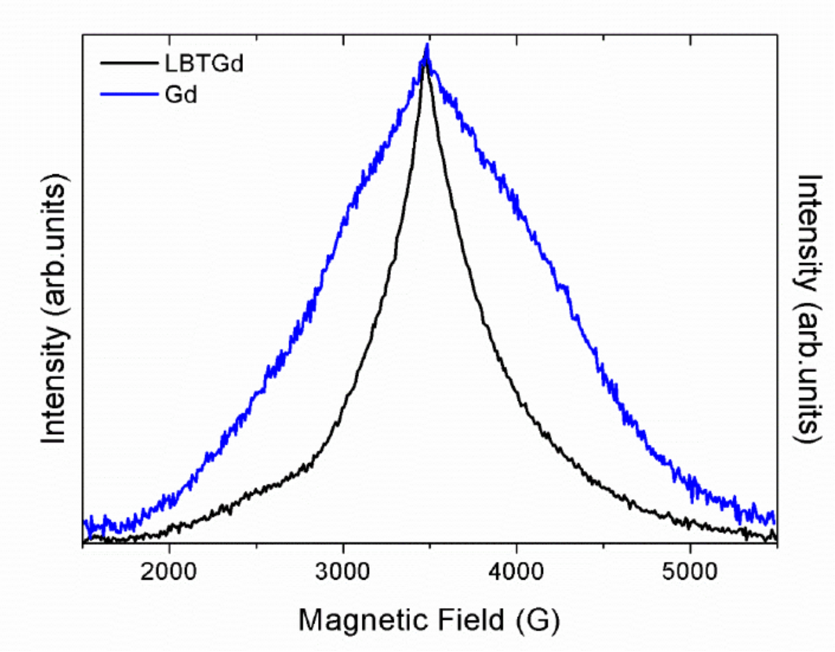

Figure S2.2. *Band echo-detected EPR as a function of magnetic field for* ***GdLBT*** *(black line) and Gd without LBT (blue line) measured at 4.5 K. Pulses of 12 ns for π/2 and 24 ns for π.*

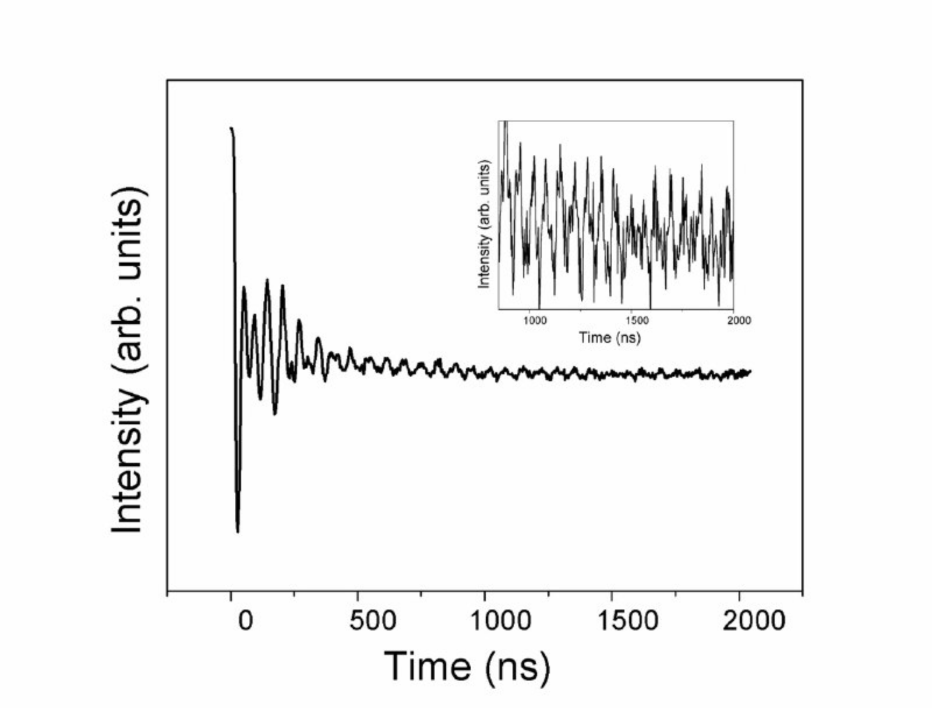

Figure S2.3. *Rabi oscillations adjusting the microwave attenuation to achieve the Hartmann-Hahn condition, (i.e. the electronic Rabi frequency matches the Larmor frequency of the proton) for a Gd sample prepared without the LBT peptide, measured at 4 K and at* B_0 *= 3480 G. Inset: zoom-in at Rabi oscillations for long times.*

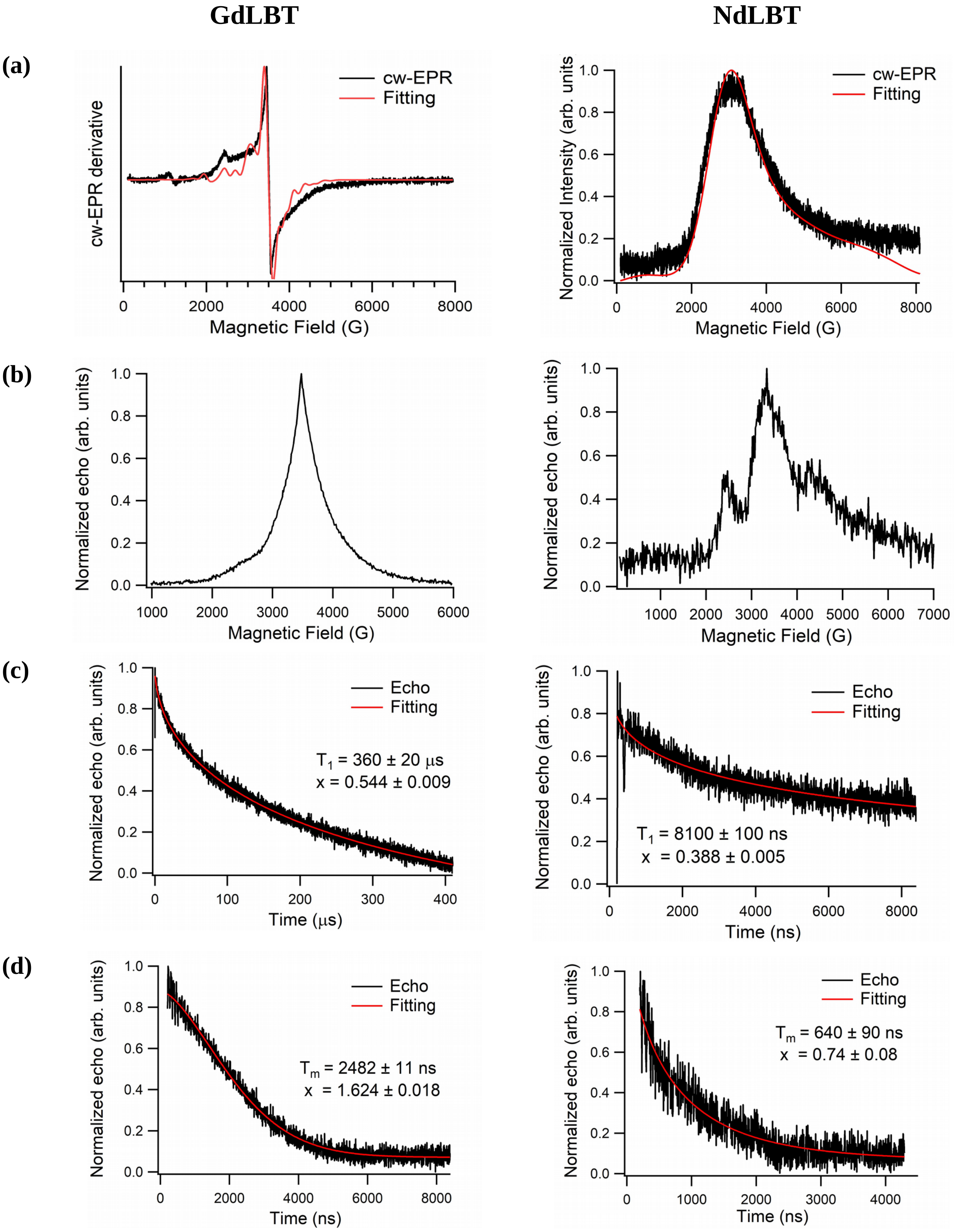

Figure S2.4. *X-band (9.71 GHz) EPR experiments at 4 K on a frozen solution of* ***LnLBT*** *(100 μM) which contained 20% Glycerol. Left:* ***GdLBT****, Right:* ***NdLBT****. (a) continuous wave EPR, (b) echo-detected EPR, (c)* T_1*, and (d)* T_m *determination. Fitting curves are monoexponential functions with stretch x.*

S3 Spin energies and spin states

The energy-level scheme and the spin states of **GdLBT** (J = 7/2) in presence of a external static magnetic field were extracted from the following spin hamiltonian:

$$\hat{\mathrm{H}} = D\left[\hat{J}_z^2 - \frac{1}{3}J\left(J+1\right)\right] + E\left(\hat{J}_x^2 - \hat{J}_y^2\right) + \mu_B g \vec{B}\cdot\vec{\hat{J}} \qquad [1]$$

The magnetic anisotropy parameters D, E and the Landé g factor, which was assumed to be isotropic, were extracted from fitting the corresponding cw-EPR spectrum (see Fig. S2.4.a left panel) by using the “pepper” package of the software EasySpin. The best fit parameters found are D = 546.6 MHz, E = 293.3 MHz, g = 2.00232. We employed isotropic D and E strains of 50 and 10 MHz respectively.

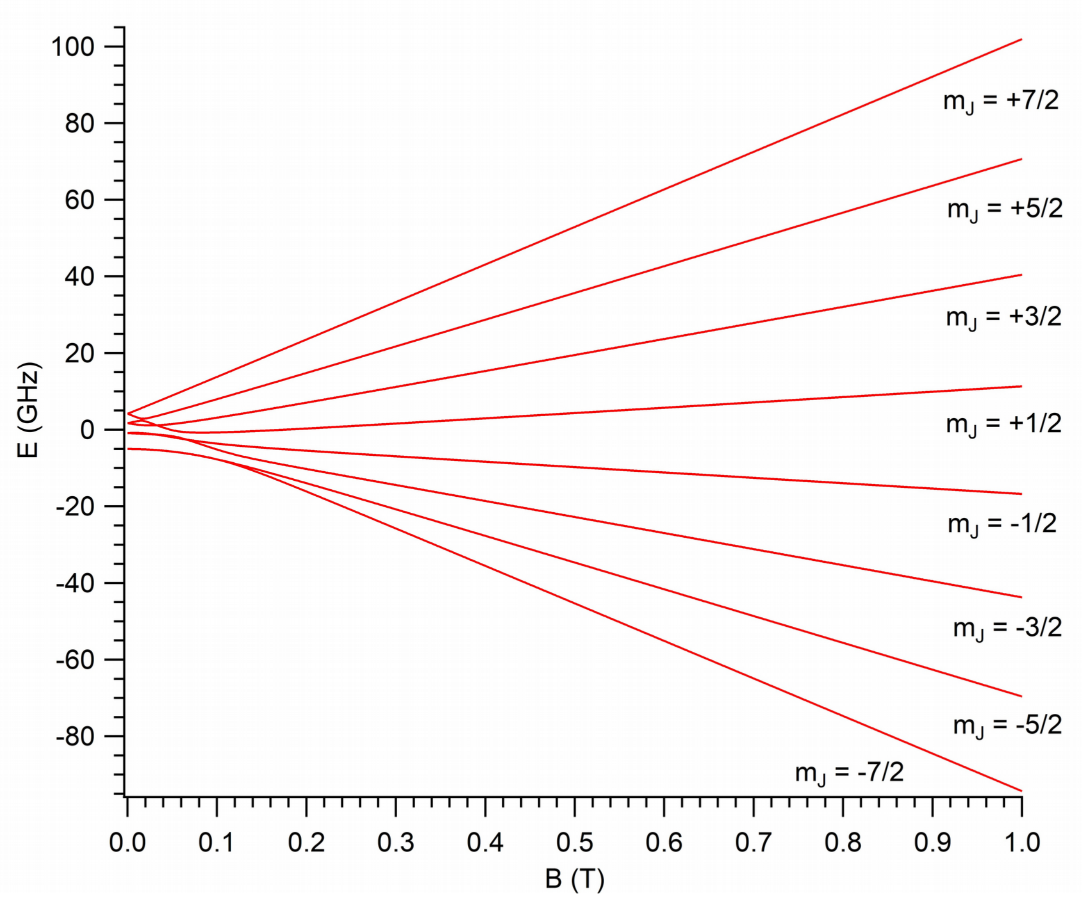

Figure S3.1. ***GdLBT*** *(J = 7/2) “Spin energies vs magnetic field” Zeeman diagram for a magnetic field applied along the z axis. Each one of the eight curves is really 4-fold degenerate as no hyperfine coupling was set in the cw-EPR fitting.*

The energy-level scheme and the spin states of **NdLBT** (J = 9/2) in presence of an external static magnetic field were extracted from the following spin Hamiltonian:

$$\hat{\mathrm{H}} = D\left[\hat{J}_z^2 - \frac{1}{3}J\left(J+1\right)\right] + \vec{\hat{J}}A\vec{\hat{I}} + \mu_B g\vec{B}\cdot\vec{\hat{J}} \qquad [2]$$

The magnetic anisotropy parameters D, $A_{\perp}$, $A_{\|}$, and the Landé g factor, which was assumed to be isotropic, were extracted from fitting the corresponding cw-EPR spectrum (see Fig. S2.4.a right panel) by using the “pepper” package of the software EasySpin. The best fit parameters found are D = -110 GHz, $A_{\perp}$ = 1.033 GHz, $A_{\|}$ = 867 MHz, g = 0.50232. No strains for D, $A_{\perp}$, $A_{\|}$, g were employed.

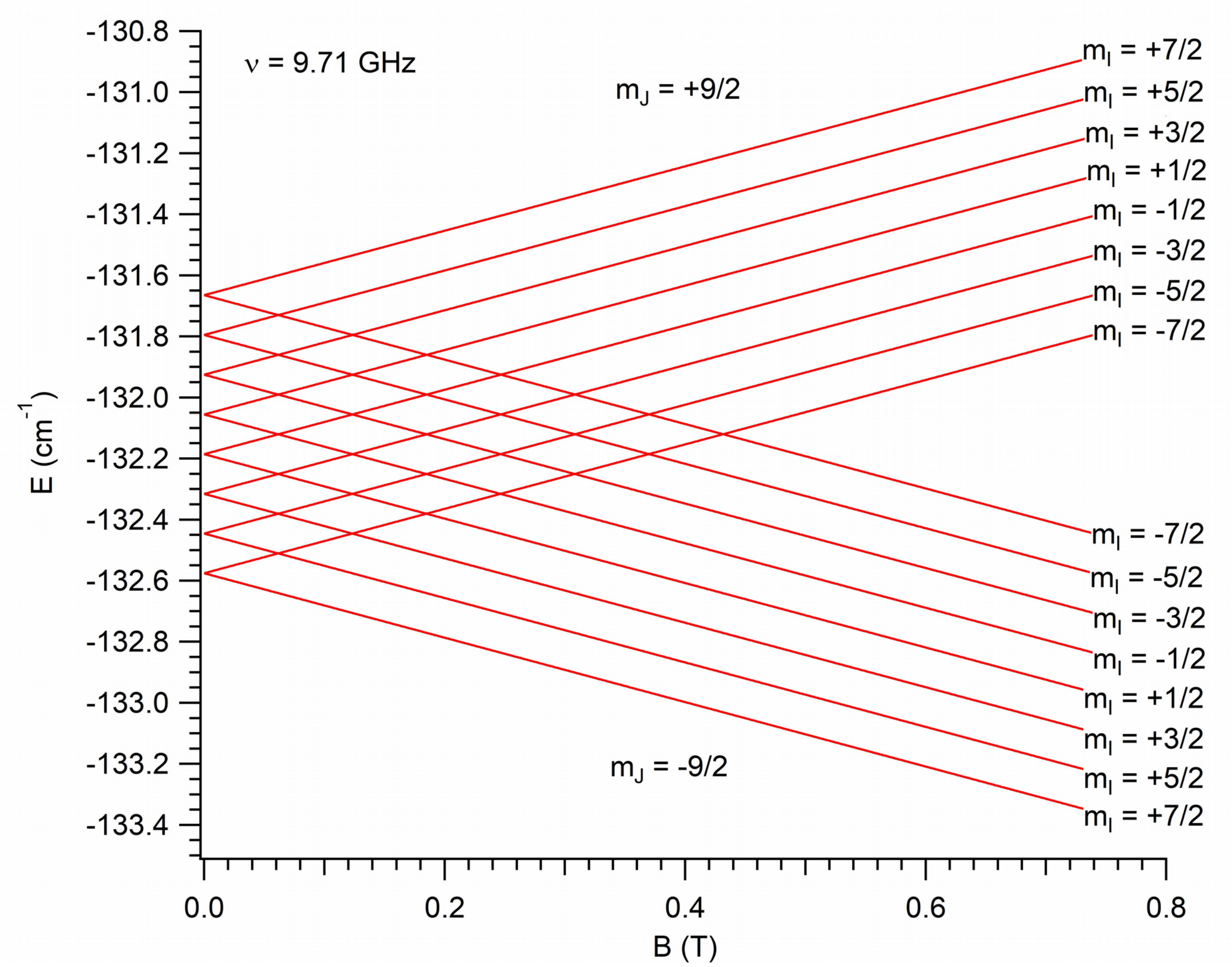

Figure S3.2. NdLBT *(J = 9/2, I = 7/2) “Spin energies vs magnetic field” Zeeman diagram of the ground doublet M_J = ± 9/2 when the magnetic field is applied along the z axis. Each component of this ground doublet is split up in the eight M_I projections of the Nd^{3+} nuclear spin due to a non-zero hyperfine coupling.*

Table S3. *Energies, wavefunctions, M_J and M_I expected values at zero magnetic field of the first sixteen **NdLBT** spin states (“ground doblet $M_J = \pm 9/2$” plus “nuclear spin manifold”) according to the Hamiltonian previously presented.*

State	Energy (MHz)	Wavefunction	Expected M_J	Expected M_I
1	0.0	(99.9998%) $\left\|-9/2,+7/2\right\rangle$	-4.499998	+3.499998
2	$2.7\cdot10^{-4}$	(99.9998%) $\left\|+9/2,-7/2\right\rangle$	+4.499998	-3.499998
3	3895.472684	(99.9996%) $\left\|-9/2,+5/2\right\rangle$	-4.499996	+2.499996
4	3895.472954	(99.9996%) $\left\|+9/2,-5/2\right\rangle$	+4.499996	-2.499996
5	7792.759087	(99.9995%) $\left\|-9/2,+3/2\right\rangle$	-4.499995	+1.499995
6	7792.759357	(99.9995%) $\left\|+9/2,-3/2\right\rangle$	+4.499995	-1.499995
7	11691.860989	(99.9995%) $\left\|-9/2,+1/2\right\rangle$	-4.499995	+0.499995
8	11691.861259	(99.9995%) $\left\|+9/2,-1/2\right\rangle$	+4.499995	-0.499995
9	15592.780171	(99.9995%) $\left\|-9/2,-1/2\right\rangle$	-4.499995	-0.500005
10	15592.780441	(99.9995%) $\left\|+9/2,+1/2\right\rangle$	+4.499995	+0.500005
11	19495.518419	(99.9996%) $\left\|-9/2,-3/2\right\rangle$	-4.499996	-1.500004
12	19495.518688	(99.9996%) $\left\|+9/2,+3/2\right\rangle$	+4.499996	+1.500004
13	23400.077517	(99.9998%) $\left\|-9/2,-5/2\right\rangle$	-4.499998	-2.500002
14	23400.077787	(99.9998%) $\left\|+9/2,+5/2\right\rangle$	+4.499998	+2.500002
15	27306.459257	(100.0000%) $\left\|-9/2,-7/2\right\rangle$	-4.500000	-3.500000
16	27306.459527	(100.0000%) $\left\|+9/2,+7/2\right\rangle$	+4.500000	+3.500000

The fitting of the cw-EPR derivative (see Fig. S3.3) in **NdLBT** was performed by considering an effective spin $J = 1/2$ and using the following spin hamiltonian in presence of an external magnetic field with anisotropic g and A tensors:

$$\hat{\mathrm{H}} = \vec{\hat{J}}\boldsymbol{A}\vec{\hat{I}} + \mu_B \vec{B} \cdot \boldsymbol{g} \cdot \vec{\hat{J}} \qquad [3]$$

The magnetic anisotropy parameters were extracted by using the “pepper” package of the software EasySpin. The best fit parameters found are A_x = -266.7 MHz, A_y = -1233 MHz, A_z = -366.7 MHz, g_x = 0.237, g_y = 0.1, g_z = 3.7. A strain of 0.6 was used in g_z.

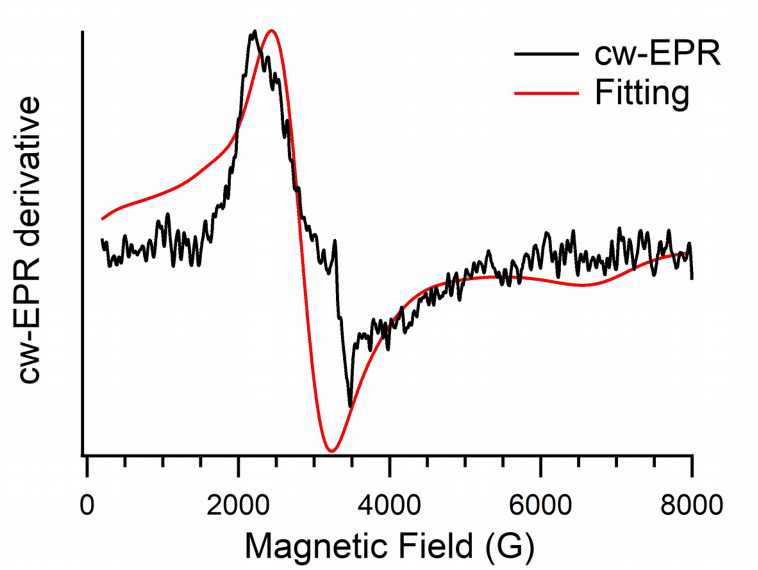

Figure S3.3. *cw-EPR derivative spectrum of* ***NdLBT*** *along with the corresponding fitting. See above for values of parameters.*

S4 Nuclear spin bath decoherence: theoretical calculations

Nuclear decoherence time T_2^n calculations were carried out by using the SIMPRE1.2 package,[10] adapted to deal with randomly oriented samples (powder or solution). The calculation was performed at a static magnetic field of 0.348 T applied along the molecular easy axis which defines the z-direction, giving a qubit gap of Δ = 9.60 GHz. This gap is close to the energy (9.71 GHz) of our X-band EPR spectrometer. The resonant transition selected, i.e., the two spin states that defines the qubit, was $|M_J = -1/2, M_I = +3/2\rangle \rightarrow |M_J = +1/2, M_I = +3/2\rangle$. There are still three more degenerate resonant transitions since no hyperfine coupling was set in the EasySpin fit, namely, $|M_J = -1/2, M_I = +1/2\rangle \rightarrow |M_J = +1/2, M_I = +1/2\rangle$, $|M_J = -1/2, M_I = -1/2\rangle \rightarrow |M_J = +1/2, M_I = -1/2\rangle$, $|M_J = -1/2, M_I = -3/2\rangle \rightarrow |M_J = +1/2, M_I = -3/2\rangle$, and they gave very similar T_2^n.

To simulate the solutions we used the PACKMOL package.[11] The **GdLBT** molecule was placed inside a sphere of a given radius R with the molecular mass centre right at the centre of the sphere. We took water (80% v/v) and glycerol (20% v/v) as the only solvents, considering that concentrations of HEPES, NaCl and β-mercaptoethanol are small enough to not have a significant importance. Herein, we considered that each atom of both, the **GdLBT** molecule and the solvents, is a sphere of radius equal to its Van der Waals radius. Then, PACKMOL randomly fills the R-radius sphere with an appropriate number of solvent molecules until reaching their relevant concentrations. In terms of number of molecules per volume, these concentrations are: $2.474 \cdot 10^{-2}$ molecules/Å^3 for water and $1.266 \cdot 10^{-3}$ molecules/Å^3 for glycerol. The magnetic nuclei positions inside the sphere is the nuclear spin bath that we took as an input for SIMPRE1.2. The radius R that we considered were 40, 50 and 60 Å, being the last one large enough to converge T_2^n. The calculated values are around 300 μs, indicating that nuclear-induced precessional decoherence is not the limiting mechanism that dephases qubit dynamics.

S5 Theoretical studies with ligand field theory.

In order to understand the influence of the ligand field around the lanthanide, which will permit the manipulation of the qubit behavior, we carried out a series of first-principles calculations using the density functional theory (DFT) package SIESTA[12] along with the SIMPRE code.[13] This allowed us to obtain a prediction of the nature of the ground state for a set of magnetic **LnLBTs**.

First, we built three LBT isomers by swapping the position of the coordinating residue *Asn3* by *Asp5 a*nd *Asp7*, alternatively. The three resulting chemical structures are:

YIDTNNDGWEGDELLA (*DND*),

YINTDNDGWEGDELLA (*NDD*) and

YIDTDNNGWEGDELLA (*DDN*).

These structures are termed DND, NDD and DDN in this section.

The next step was to relax these molecular structures while coordinating a Ca^{2+} atom (we decided to use Ca^{2+} instead of a Ln^{3+} for computational simplicity and to avoid the spin degrees of freedom in the relaxation step). The CaLBT molecular structure was fully optimized using the SIESTA code, until the maximum atomic forces were less than 0.01 eV/Å. A real space grid with an equivalent plane wave cutoff of 200 Ry –enough to ensure convergence– has been used to calculate the various matrix elements. The obtained relaxed structures may be observed in Fig. 5.1.

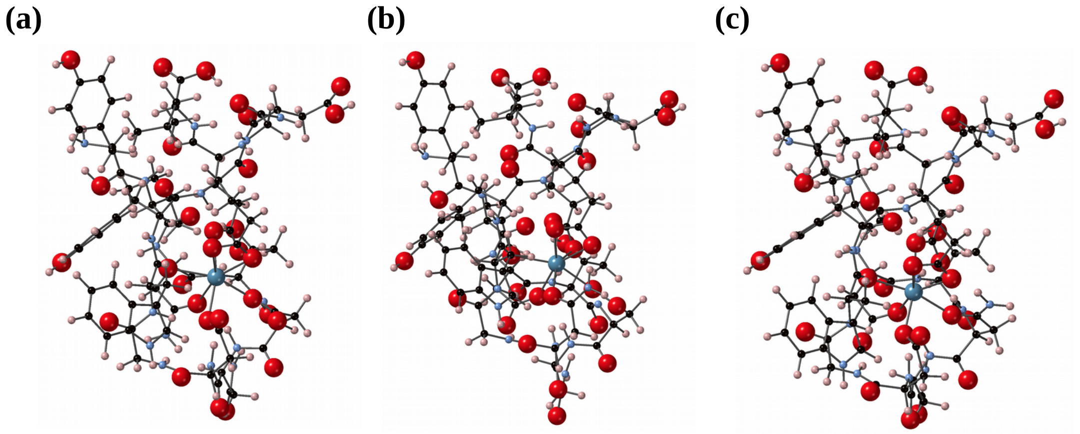

Figure S5.1. *Ball&stick representation of the relaxed molecular structures of (a) Ca@DND, (b) Ca@DDN and (c) Ca@NDD.*

As can be seen in these depictions, the main secondary structure of the polypeptide remains practically unaltered, i.e. it has not been affected by changes on the coordination environment around the lanthanoid. We used these three coordination schemes, which belong to robust structures, to explore the effect of different donor atoms on the ground state description using the SIMPRE computational package. As a first step, we have defined three types of coordination oxygen atoms: (a) those that come from a monocoordinated carboxylate ligand (Asp[3, 5, 7], which has a formal charge of -1.0), (b) those arising from a bicoordinated carboxylate ligand (Glu11 & Glu14, with a formal charge -0.5) and (c) those corresponding to formally uncharged oxygens (Trp(9), Asn[3, 5, 7], formal charge 0.0). A similar approach, using formal charges and the original point charge electrostatic model (PCEM), was implemented to investigate magnetic anisotropy on Dy complexes.[14] In this work, we improve this strategy by using the Radial Effective Charge (REC) model, which incorporates covalent effects through the radial displacement parameter (D_r) and its corresponding effective charge (Z_i) (See Figure S4.2). [15]

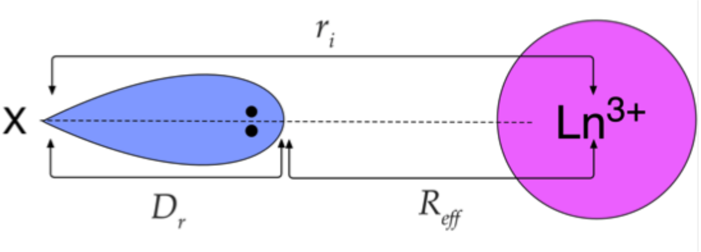

Figure S5.2. *Electronic pair of a ligand X oriented towards the nucleus of a trivalent lanthanoid cation. The effective charge is located between the lanthanoid and the donor atom at* $R_{eff} = R_i - D_r$.

In a first step, we start the qualitative exploration by sampling a few ratios for the parameters D_r and Z_i. Three different sets of REC parameters were defined (see Table 5.3), corresponding to rising estimates of the covalency effect. This allowed us to discriminate and select only robust results, where the connection between peptidic sequence and nature of the ground state is not dependent on our parameter choice. One can observe that the REC parameters of the atoms with formal charge -1.0 are equivalent for all three sets. They have been extracted from previous works where they were successfully used to describe the properties of either oxo atoms from a polyoxometalate ligand[16] or hydroxy (OH^-) ligands.[17] In the other two cases –formal charges -0.5 and 0.0–, we have considered three different possibilities, always keeping constant the total $D_r{\cdot}Z_i$ product.[18] To obtain an approximated order of magnitude, we considered the REC parameters (D_r = 1.1 Å and Z_i = 0.085) which reproduced the spectroscopic energy levels of a system coordinated by the bidentate ligand oxydiacetate (ODA).[19] In this latter case, the donor atoms are of similar nature than the ones of our case (carboxylates and carbonyl groups), having an average formal charge of -2/3.

Table S5.3. *Description of the different parameter sets used in the calculations. Each ligand described by its formal charge (-1.0, -0.5 or 0.0) has a* D_r */*Z_i *value correspondence.*

Formal Charge	**Mode 1**		**Mode 2**		**Mode 3**	
	D_r (Å)	**Zi**	**D_r (Å)**	**Z_i**	**D_r (Å)**	**Z_i**
-1.0	0.895	0.105	0.895	0.105	0.895	0.105
-0.5	1.04	0.090	1.10	0.085	1.22	0.076
0.0	1.22	0.076	1.35	0.069	1.66	0.056

Table S5.4. *Explicit wavefunction for each studied lanthanoid ion, in the mode 1 for the modified peptide NDD.*

mode1																	
Nd@NDD	-9/2	-7/2	-5/2	-3/2	-1/2	1/2	3/2	5/2	7/2	9/2							
	0.030	0.037	0.708	0.035	0.016	0.000	0.153	0.006	0.014	0.001							
mode1																	
Tb@NDD	-6	-5	-4	-3	-2	-1	0	1	2	3	4	5	6				
	0.007	0.003	0.010	0.051	0.117	0.000	0.625	0.000	0.117	0.051	0.010	0.003	0.007				
mode1																	
Dy@NDD	-15/2	-13/2	-11/2	-9/2	-7/2	-5/2	-3/2	-1/2	1/2	3/2	5/2	7/2	9/2	11/2	13/2	15/2	
	0.968	0.000	0.024	0.002	0.003	0.001	0.001	0.000	0.000	0.000	0.000	0.000	0.000	0.000	0.000	0.000	
mode1																	
Ho@NDD	-8	-7	-6	-5	-4	-3	-2	-1	0	1	2	3	4	5	6	7	8
	0.000	0.004	0.001	0.006	0.015	0.003	0.213	0.000	0.516	0.000	0.213	0.003	0.015	0.006	0.001	0.004	0.000
mode1																	
Er@NDD	-15/2	-13/2	-11/2	-9/2	-7/2	-5/2	-3/2	-1/2	1/2	3/2	5/2	7/2	9/2	11/2	13/2	15/2	
	0.044	0.695	0.024	0.012	0.016	0.073	0.042	0.061	0.007	0.019	0.002	0.000	0.001	0.002	0.000	0.000	
mode1																	
Tm@NDD	-6	-5	-4	-3	-2	-1	0	1	2	3	4	5	6				
	0.020	0.058	0.011	0.049	0.072	0.000	0.579	0.000	0.072	0.049	0.011	0.058	0.020				
mode1																	
Yb@NDD	-7/2	-5/2	-3/2	-1/2	1/2	3/2	5/2	7/2									
	0.008	0.009	0.011	0.877	0.007	0.041	0.003	0.044									

Table S5.5. *Explicit wavefunction for each studied lanthanoid ion, in the mode 2 for the modified peptide NDD.*

mode2																	
Nd@NDD	-9/2	-7/2	-5/2	-3/2	-1/2	1/2	3/2	5/2	7/2	9/2							
	0.057	0.031	0.672	0.029	0.017	0.000	0.174	0.005	0.013	0.000							
mode2																	
Tb@NDD	-6	-5	-4	-3	-2	-1	0	1	2	3	4	5	6				
	0.027	0.002	0.009	0.008	0.158	0.000	0.592	0.000	0.158	0.008	0.009	0.002	0.027				
mode2																	
Dy@NDD	-15/2	-13/2	-11/2	-9/2	-7/2	-5/2	-3/2	-1/2	1/2	3/2	5/2	7/2	9/2	11/2	13/2	15/2	
	0.912	0.000	0.065	0.011	0.005	0.002	0.002	0.001	0.001	0.000	0.000	0.000	0.000	0.000	0.000	0.000	
mode2																	
Ho@NDD	-8	-7	-6	-5	-4	-3	-2	-1	0	1	2	3	4	5	6	7	8
	0.000	0.003	0.000	0.008	0.012	0.005	0.200	0.000	0.542	0.000	0.200	0.005	0.012	0.008	0.000	0.003	0.000
mode2																	
Er@NDD	-15/2	-13/2	-11/2	-9/2	-7/2	-5/2	-3/2	-1/2	1/2	3/2	5/2	7/2	9/2	11/2	13/2	15/2	
	0.019	0.810	0.010	0.013	0.008	0.019	0.018	0.064	0.008	0.014	0.000	0.000	0.001	0.015	0.000	0.001	
mode2																	
Tm@NDD	-6	-5	-4	-3	-2	-1	0	1	2	3	4	5	6				
	0.034	0.089	0.006	0.058	0.040	0.000	0.547	0.000	0.040	0.058	0.006	0.089	0.034				
mode2																	
Yb@NDD	-7/2	-5/2	-3/2	-1/2	1/2	3/2	5/2	7/2									
	0.004	0.015	0.003	0.903	0.004	0.035	0.002	0.035									

Table S5.6. *Explicit wavefunction for each studied lanthanoid ion, in the mode 3 for the modified peptide NDD.*

mode3																	
Nd@NDD	-9/2	-7/2	-5/2	-3/2	-1/2	1/2	3/2	5/2	7/2	9/2							
	0.207	0.001	0.694	0.001	0.014	0.001	0.079	0.001	0.003	0.000							
mode3																	
Tb@DD	-6	-5	-4	-3	-2	-1	0	1	2	3	4	5	6				
	0.034	0.063	0.006	0.075	0.024	0.000	0.597	0.000	0.024	0.075	0.006	0.063	0.034				
mode3																	
Dy@NDD	-15/2	-13/2	-11/2	-9/2	-7/2	-5/2	-3/2	-1/2	1/2	3/2	5/2	7/2	9/2	11/2	13/2	15/2	
	0.005	0.759	0.003	0.002	0.000	0.009	0.011	0.168	0.009	0.028	0.002	0.000	0.000	0.003	0.000	0.001	
mode3																	
Ho@NDD	-8	-7	-6	-5	-4	-3	-2	-1	0	1	2	3	4	5	6	7	8
	0.000	0.015	0.004	0.011	0.007	0.010	0.179	0.000	0.548	0.000	0.179	0.010	0.007	0.011	0.004	0.015	0.000
mode3																	
Er@NDD	-15/2	-13/2	-11/2	-9/2	-7/2	-5/2	-3/2	-1/2	1/2	3/2	5/2	7/2	9/2	11/2	13/2	15/2	
	0.001	0.945	0.000	0.007	0.004	0.010	0.004	0.024	0.000	0.003	0.000	0.000	0.000	0.001	0.000	0.000	
mode3																	
Tm@NDD	-6	-5	-4	-3	-2	-1	0	1	2	3	4	5	6				
	0.014	0.146	0.000	0.094	0.000	0.000	0.490	0.000	0.000	0.094	0.000	0.146	0.014				
mode3																	
Yb@NDD	-7/2	-5/2	-3/2	-1/2	1/2	3/2	5/2	7/2									
	0.001	0.074	0.001	0.883	0.002	0.021	0.001	0.016									

Table S5.7. *Explicit wavefunction for each studied lanthanoid ion, in the mode 1 for the modified peptide DND.*

mode1																	
Nd@DND	-9/2	-7/2	-5/2	-3/2	-1/2	1/2	3/2	5/2	7/2	9/2							
	0.818	0.000	0.126	0.023	0.000	0.011	0.021	0.001	0.000	0.000							
mode1																	
Tb@DND	-6	-5	-4	-3	-2	-1	0	1	2	3	4	5	6				
	0.000	0.000	0.017	0.000	0.228	0.000	0.511	0.000	0.228	0.000	0.017	0.000	0.000				
mode1																	
Dy@DND	-15/2	-13/2	-11/2	-9/2	-7/2	-5/2	-3/2	-1/2	1/2	3/2	5/2	7/2	9/2	11/2	13/2	15/2	
	0.989	0.000	0.009	0.001	0.000	0.000	0.000	0.000	0.000	0.000	0.000	0.000	0.000	0.000	0.000	0.000	
mode1																	
Ho@DND	-8	-7	-6	-5	-4	-3	-2	-1	0	1	2	3	4	5	6	7	8
	0.494	0.000	0.004	0.001	0.000	0.001	0.000	0.000	0.000	0.000	0.000	0.001	0.000	0.001	0.004	0.000	0.494
mode1																	
Er@DND	-15/2	-13/2	-11/2	-9/2	-7/2	-5/2	-3/2	-1/2	1/2	3/2	5/2	7/2	9/2	11/2	13/2	15/2	
	0.005	0.008	0.196	0.008	0.007	0.001	0.001	0.611	0.003	0.002	0.006	0.001	0.111	0.003	0.025	0.012	
mode1																	
Tm@DND	-6	-5	-4	-3	-2	-1	0	1	2	3	4	5	6				
	0.007	0.018	0.011	0.076	0.055	0.000	0.664	0.000	0.055	0.076	0.011	0.018	0.007				
mode1																	
Yb@DND	-7/2	-5/2	-3/2	-1/2	1/2	3/2	5/2	7/2									
	0.006	0.023	0.000	0.949	0.000	0.020	0.000	0.002									

Table S5.8. *Explicit wavefunction for each studied lanthanoid ion, in the mode 2 for the modified peptide DND.*

mode2																	
Nd@DND	-9/2	-7/2	-5/2	-3/2	-1/2	1/2	3/2	5/2	7/2	9/2							
	0.100	0.772	0.056	0.031	0.025	0.009	0.005	0.002	0.000	0.000							
mode2																	
Tb@DND	-6	-5	-4	-3	-2	-1	0	1	2	3	4	5	6				
	0.000	0.000	0.017	0.000	0.227	0.000	0.511	0.000	0.227	0.000	0.017	0.000	0.000				
mode2																	
Dy@DND	-15/2	-13/2	-11/2	-9/2	-7/2	-5/2	-3/2	-1/2	1/2	3/2	5/2	7/2	9/2	11/2	13/2	15/2	
	0.990	0.000	0.009	0.001	0.000	0.000	0.000	0.000	0.000	0.000	0.000	0.000	0.000	0.000	0.000	0.000	
mode2																	
Ho@DND	-8	-7	-6	-5	-4	-3	-2	-1	0	1	2	3	4	5	6	7	8
	0.49	0.00	0.00	0.00	0.00	0.00	0.00	0.00	0.00	0.00	0.00	0.00	0.00	0.00	0.00	0.00	0.49
mode2																	
Er@DND	-15/2	-13/2	-11/2	-9/2	-7/2	-5/2	-3/2	-1/2	1/2	3/2	5/2	7/2	9/2	11/2	13/2	15/2	
	0.013	0.893	0.007	0.003	0.002	0.001	0.042	0.031	0.005	0.001	0.000	0.000	0.000	0.004	0.000	0.000	
mode2																	
Tm@DND	-6	-5	-4	-3	-2	-1	0	1	2	3	4	5	6				
	0.014	0.033	0.007	0.106	0.023	0.000	0.635	0.000	0.023	0.106	0.007	0.033	0.014				
mode2																	
Yb@DND	-7/2	-5/2	-3/2	-1/2	1/2	3/2	5/2	7/2									
	0.004	0.014	0.000	0.972	0.000	0.007	0.000	0.002									

Table S5.9. *Explicit wavefunction for each studied lanthanoid ion, in the mode 3 for the modified peptide DND.*

mode3																	
Nd@DND	-9/2	-7/2	-5/2	-3/2	-1/2	1/2	3/2	5/2	7/2	9/2							
	0.017	0.718	0.010	0.016	0.002	0.072	0.003	0.122	0.000	0.039							
mode3																	
Tb@DND	-6	-5	-4	-3	-2	-1	0	1	2	3	4	5	6				
	0.001	0.002	0.046	0.005	0.136	0.000	0.620	0.000	0.136	0.005	0.046	0.002	0.001				
mode3																	
Dy@DND	-15/2	-13/2	-11/2	-9/2	-7/2	-5/2	-3/2	-1/2	1/2	3/2	5/2	7/2	9/2	11/2	13/2	15/2	
	0.956	0.000	0.036	0.001	0.004	0.001	0.002	0.000	0.000	0.000	0.000	0.000	0.000	0.000	0.000	0.000	
mode3																	
Ho@DND	-8	-7	-6	-5	-4	-3	-2	-1	0	1	2	3	4	5	6	7	8
	0.002	0.004	0.052	0.003	0.044	0.019	0.064	0.000	0.625	0.000	0.064	0.019	0.044	0.003	0.052	0.004	0.002
mode3																	
Er@DND	-15/2	-13/2	-11/2	-9/2	-7/2	-5/2	-3/2	-1/2	1/2	3/2	5/2	7/2	9/2	11/2	13/2	15/2	
	0.008	0.792	0.005	0.001	0.010	0.007	0.055	0.086	0.013	0.002	0.002	0.000	0.001	0.019	0.000	0.000	
mode3																	
Tm@DND	-6	-5	-4	-3	-2	-1	0	1	2	3	4	5	6				
	0.020	0.061	0.015	0.099	0.060	0.000	0.491	0.000	0.060	0.099	0.015	0.061	0.020				
mode3																	
Yb@DND	-7/2	-5/2	-3/2	-1/2	1/2	3/2	5/2	7/2									
	0.817	0.000	0.034	0.027	0.065	0.004	0.053	0.000									

Table S5.10. *Explicit wavefunction for each studied lanthanoid ion, in the mode 1 for the modified peptide DNN.*

mode1																
Nd@DDN	-9/2	-7/2	-5/2	-3/2	-1/2	1/2	3/2	5/2	7/2	9/2						
	0.034	0.694	0.024	0.025	0.033	0.015	0.013	0.129	0.009	0.025						
mode1																
Tb@DDN	-6	-5	-4	-3	-2	-1	0	1	2	3	4	5	6			
	0.005	0.005	0.000	0.030	0.155	0.000	0.608	0.000	0.155	0.030	0.000	0.005	0.005			
mode1																
Dy@DDN	-15/2	-13/2	-11/2	-9/2	-7/2	-5/2	-3/2	-1/2	1/2	3/2	5/2	7/2	9/2	11/2	13/2	15/2	
	0.973	0.000	0.012	0.002	0.005	0.000	0.005	0.000	0.002	0.000	0.000	0.000	0.000	0.000	0.000	0.000	
mode1																
Ho@DDN	-8	-7	-6	-5	-4	-3	-2	-1	0	1	2	3	4	5	6	7	8
	0.000	0.002	0.006	0.003	0.035	0.007	0.188	0.000	0.519	0.000	0.188	0.007	0.035	0.003	0.006	0.002	0.000
mode1																
Er@DDN	-15/2	-13/2	-11/2	-9/2	-7/2	-5/2	-3/2	-1/2	1/2	3/2	5/2	7/2	9/2	11/2	13/2	15/2	
	0.011	0.038	0.693	0.027	0.035	0.004	0.020	0.004	0.093	0.005	0.002	0.000	0.008	0.005	0.055	0.000	
mode1																
Tm@DDN	-6	-5	-4	-3	-2	-1	0	1	2	3	4	5	6			
	0.018	0.028	0.004	0.070	0.054	0.000	0.653	0.000	0.054	0.070	0.004	0.028	0.018			
mode1																
Yb@DDN	-7/2	-5/2	-3/2	-1/2	1/2	3/2	5/2	7/2								
	0.084	0.024	0.028	0.746	0.036	0.050	0.005	0.026								

Table S5.11. *Explicit wavefunction for each studied lanthanoid ion, in the mode 2 for the modified peptide DNN.*

mode2																	
Nd@DDN	-9/2	-7/2	-5/2	-3/2	-1/2	1/2	3/2	5/2	7/2	9/2							
	0.254	0.016	0.005	0.000	0.714	0.000	0.006	0.004	0.001	0.000							
mode2																	
Tb@DDN	-6	-5	-4	-3	-2	-1	0	1	2	3	4	5	6				
	0.024	0.004	0.005	0.038	0.138	0.000	0.582	0.000	0.138	0.038	0.005	0.004	0.024				
mode2																	
Dy@DDN	-15/2	-13/2	-11/2	-9/2	-7/2	-5/2	-3/2	-1/2	1/2	3/2	5/2	7/2	9/2	11/2	13/2	15/2	
	0.959	0.000	0.020	0.001	0.006	0.000	0.009	0.001	0.004	0.000	0.000	0.000	0.000	0.000	0.000	0.000	
mode2																	
Ho@DDN	-8	-7	-6	-5	-4	-3	-2	-1	0	1	2	3	4	5	6	7	8
	0.000	0.006	0.013	0.003	0.039	0.012	0.166	0.000	0.522	0.000	0.166	0.012	0.039	0.003	0.013	0.006	0.000
mode2																	
Er@DDN	-15/2	-13/2	-11/2	-9/2	-7/2	-5/2	-3/2	-1/2	1/2	3/2	5/2	7/2	9/2	11/2	13/2	15/2	
	0.102	0.014	0.085	0.009	0.602	0.010	0.003	0.005	0.025	0.000	0.121	0.006	0.017	0.000	0.000	0.001	
mode2																	
Tm@DDN	-6	-5	-4	-3	-2	-1	0	1	2	3	4	5	6				
	0.024	0.054	0.002	0.094	0.022	0.000	0.610	0.000	0.022	0.094	0.002	0.054	0.024				
mode2																	
Yb@DDN	-7/2	-5/2	-3/2	-1/2	1/2	3/2	5/2	7/2									
	0.001	0.008	0.071	0.772	0.032	0.011	0.004	0.101									

Table S5.12. *Explicit wavefunction for each studied lanthanoid ion, in the mode 3 for the modified peptide DNN.*

mode3																	
Nd@DDN	-9/2	-7/2	-5/2	-3/2	-1/2	1/2	3/2	5/2	7/2	9/2							
	0.303	0.000	0.012	0.000	0.647	0.000	0.002	0.000	0.036	0.000							
mode3																	
Tb@DDN	-6	-5	-4	-3	-2	-1	0	1	2	3	4	5	6				
	0.002	0.007	0.261	0.006	0.001	0.000	0.444	0.000	0.001	0.006	0.261	0.007	0.002				
mode3																	
Dy@DDN	-15/2	-13/2	-11/2	-9/2	-7/2	-5/2	-3/2	-1/2	1/2	3/2	5/2	7/2	9/2	11/2	13/2	15/2	
	0.005	0.389	0.002	0.007	0.000	0.005	0.003	0.539	0.003	0.006	0.000	0.000	0.000	0.032	0.000	0.007	
mode3																	
Ho@DDN	-8	-7	-6	-5	-4	-3	-2	-1	0	1	2	3	4	5	6	7	8
	0.000	0.026	0.075	0.001	0.031	0.044	0.055	0.000	0.534	0.000	0.055	0.044	0.031	0.001	0.075	0.026	0.000
mode3																	
Er@DDN	-15/2	-13/2	-11/2	-9/2	-7/2	-5/2	-3/2	-1/2	1/2	3/2	5/2	7/2	9/2	11/2	13/2	15/2	
	0.001	0.809	0.000	0.000	0.001	0.019	0.003	0.129	0.000	0.003	0.000	0.000	0.000	0.033	0.000	0.000	
mode3																	
Tm@DDN	-6	-5	-4	-3	-2	-1	0	1	2	3	4	5	6				
	0.000850	0.000114	0.000694	0.493303	0.000576	0.004463	0.000000	0.004463	0.000576	0.493303	0.000694	0.000114	0.000850				
mode3																	
Yb@DDN	-7/2	-5/2	-3/2	-1/2	1/2	3/2	5/2	7/2									
	0.047495	0.003151	0.065626	0.674942	0.072681	0.060422	0.009315	0.066369									

After a first initial sampling using these discrete sets, we decided that a promising control of the qubit behavior could be performed in the Nd^{3+} derivative, as we find that its ground state can be rationally controlled by specific changes in the peptidic sequences: we obtained that an NDD environment consistently produces a different M_J in the ground doublet compared with DND. For the other metals the sampling was either inconclusive or indicated a constant ground doublet independently of the position of the aspartate/arginine residues. Thus, we prepared a new set of continuous calculations with a fine-grained variation of the covalence parameters (D_r). These calculations were performed for both Nd^{3+} and Er^{3+}, using the latter as an example of a ground doublet that seems unmodified with the structural changes.

Thus we maintained a constant ratio D_r/Z_i and varied D_r between two reasonable limits of covalence. The results obtained from this exhaustive exploration are described in the main text (see Fig. 3).

The REC parameters D_r and Z_i are obtained using the following equations:

$$Z_i(-1.0) = 0.105 \qquad [4]$$

$$Z_i(0.0) = 0.065 \bullet 1.0154^n \qquad [5]$$

$$Z_i(-0.5) = 0.083 \bullet 1.0085^n \qquad [6]$$

with n variiying between 0 and 20, while D_r for all cases is obtained for $D_r \cdot Z_i = 0.093$.

S6 Steps for the design of a low spin-vibrational-coupling peptidic spin

A major advantage of using peptidic spin qubits as building blocks for spintronics is the possibility for systematic property optimization: whether one is interested in quantum coherence or in any other specific spintronic effect, the rational procedure to improve the desired property would be to perform a screening of a combinatorial peptide library, i.e. to make combinations of substitutions of individual aminoacids in the sequence to obtain progressively better properties.

In this case, we suggest one would proceed as follows:

In a first phase, on would employ an inexpensive approach such as Force Fields (e.g. using the Amber suite) to estimate the molecular vibrations of a given peptidic spin qubit. With a set of normal vibrational modes, it is then possible to generate a set of distorted geometries, following each of these normal modes. One would perform an energy cutoff discarding all vibrational modes above 300 K and thus greatly simplifying the problem, since there is no interest in calculating the high-energy modes which will not be populated at any reasonable temperatures. One would then calculate the energy of the spin qubit, corresponding in our case to the magnetic levels of the ground NdLBT doublet at the operating magnetic field. This can be done inexpensively employing an effective electrostatic approach such as the REC model with SIMPRE or with more care by ab initio methods (MOLCAS or ORCA). As presented recently in Escalera-Moreno *et al.*[20] this is enough to determine the set of key local vibrations in the relaxation of a molecular spin qubit (or a single-molecule magnet).

The second phase of the work would involve designing a peptidic library, based on the original peptidic spin qubit. From the first phase one can determine, for the vibrations that are key for spin relaxations, which are the aminoacids with the greatest displacement. Moreover, one can also determine which are the aminoacid-aminoacid distances that are most affected by these key vibrations. Exploring controlled changes in precisely these two sets of aminoacids should guide the design of the peptidic library, which can then be systematically explored. From the point of view of the experiment and to save time, we suggest that it is enough for each peptide to do a relatively inexpensive test by means of an quick EPR experiment, such as determining the presence and intensity of a spin echo at 100 K, which does not require the time- (and resource-) intensive task of cooling the system to liquid He temperatures. This would allow exploring many samples a day.

S7 Crystallization attempts of the LBT peptide

Crystallography of LBT proved challenging. Peptide crystallization was pursued by the vapor diffusion method using the sitting drop technique by mixing 0.4 µl of peptide (2.5 and 5 mg/ml in 10 mM HEPES and 1.2 mM $TbCl_3$ pH 7.0) with 0.4 µl of different reservoir solutions in 96-well MRC-type crystallization plates. Reservoir solutions were based on previous reported crystallization conditions (3.7 mM NaCl, 100 mM Tris at pH 6.5 and 40% t-butanol) as well as in different sparse matrix screens.[2] Sparse matrix screens used for peptide crystallization were JBScreen Classic HTS I and II, JBScreen JCSG++ and JBScreen PACT++ from Jena Bioscience (Germany). We tested all resulting crystals at the synchrotrons Alba (Barcelona, Spain) and Diamond Light Source (Didcot, UK), but in every case they corresponded to salts. Thus, we were unable to reproduce the previous reported crystals obtained by the microbatch technique.

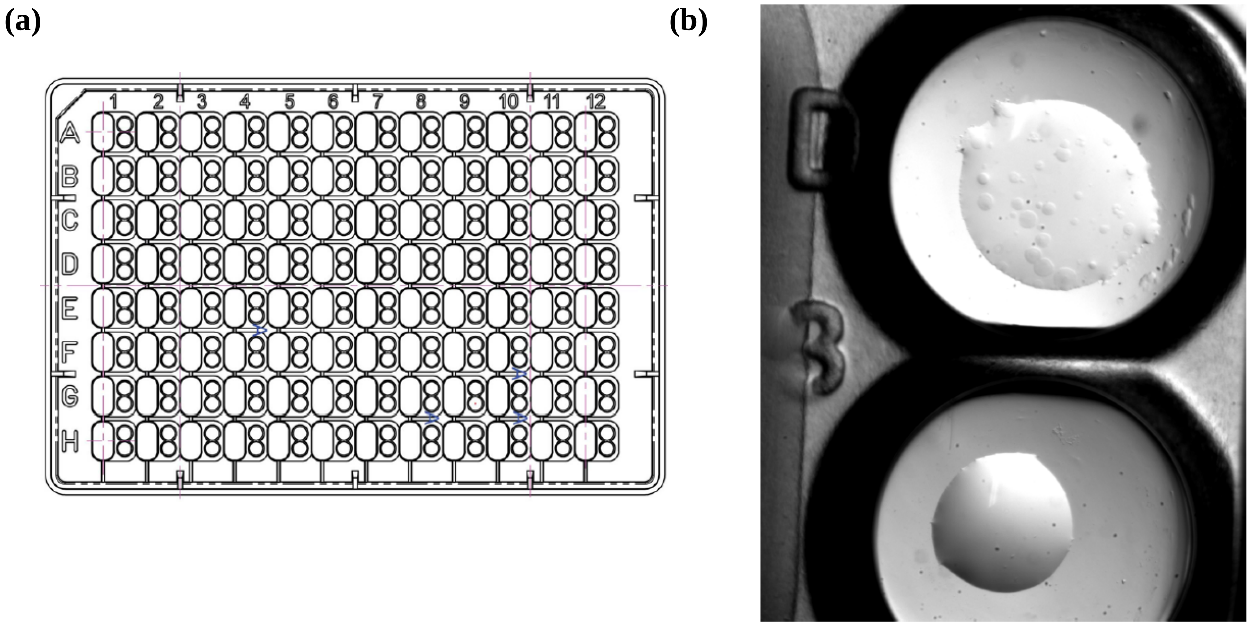

Figure S7. *(a) Scheme of the typical MRC-type plate we used for crystallization assays. (b) View of a pair of wells with spherulites in one of them from one of our assays.*

References

(1) Nitz, M.; Franz, K. J.; Maglathlin, R. L.; Imperiali, B. A Powerful Combinatorial Screen to Identify High-Affinity Terbium(III)-Binding Peptides. *Chembiochem Eur. J. Chem. Biol.* **2003**, *4* (4), 272–276.

(2) Nitz, M.; Sherawat, M.; Franz, K. J.; Peisach, E.; Allen, K. N.; Imperiali, B. Structural Origin of the High Affinity of a Chemically Evolved Lanthanide-Binding Peptide. *Angew. Chem. Int. Ed Engl.* **2004**, *43* (28), 3682–3685.

(3) Silvaggi, N. R.; Martin, L. J.; Schwalbe, H.; Imperiali, B.; Allen, K. N. Double-Lanthanide-Binding Tags for Macromolecular Crystallographic Structure Determination. *J. Am. Chem. Soc.* **2007**, *129* (22), 7114–7120.

(4) Barthelmes, K.; Reynolds, A. M.; Peisach, E.; Jonker, H. R. A.; DeNunzio, N. J.; Allen, K. N.; Imperiali, B.; Schwalbe, H. Engineering Encodable Lanthanide-Binding Tags into Loop Regions of Proteins. *J. Am. Chem. Soc.* **2011**, *133* (4), 808–819.

(5) Daughtry, K. D.; Martin, L. J.; Sarraju, A.; Imperiali, B.; Allen, K. N. Tailoring Encodable Lanthanide-Binding Tags as MRI Contrast Agents. *Chembiochem Eur. J. Chem. Biol.* **2012**, *13* (17), 2567–2574.

(6) Barb, A. W.; Ho, T. G.; Flanagan-Steet, H.; Prestegard, J. H. Lanthanide Binding and IgG Affinity Construct: Potential Applications in Solution NMR, MRI, and Luminescence Microscopy. *Protein Sci. Publ. Protein Soc.* **2012**, *21* (10), 1456–1466.

(7) Alvarez, S.; Alemany, P.; Casanova, D.; Cirera, J.; Llunell, M.; Avnir, D. Shape Maps and Polyhedral Interconversion Paths in Transition Metal Chemistry. *Coord. Chem. Rev.* **2005**, *249* (17), 1693–1708.

(8) Gurusaran, M.; Shankar, M.; Nagarajan, R.; Helliwell, J. R.; Sekar, K. Do We See What We Should See? Describing Non-Covalent Interactions in Protein Structures Including Precision. *IUCrJ* **2014**, *1* (Pt 1), 74–81.

(9) Hirsh, D. J.; Brudvig, G. W. Measuring Distances in Proteins by Saturation-Recovery EPR. *Nat. Protoc.* **2007**, *2* (7), 1770–1781.

(10) Cardona-Serra, S.; Escalera-Moreno, L.; Baldoví, J. J.; Gaita-Ariño, A.; Clemente-Juan, J. M.; Coronado, E. SIMPRE1.2: Considering the Hyperfine and Quadrupolar Couplings and the Nuclear Spin Bath Decoherence. *J. Comput. Chem.* **2016**, *37* (13), 1238–1244.

(11) Martínez, L.; Andrade, R.; Birgin, E. G.; Martínez, J. M. PACKMOL: A package for building initial configurations for molecular dynamics simulations. *J. Comput. Chem. 30* (13), 2157–2164.

(12) Soler, J. M.; Artacho, E.; Gale, J. D.; García, A.; Junquera, J.; Ordejón, P.; Daniel Sánchez-Portal. The SIESTA Method for Ab Initio Order- N Materials Simulation. *J. Phys. Condens. Matter* **2002**, *14* (11), 2745.

(13) Baldoví, J. J.; Cardona-Serra, S.; Clemente-Juan, J. M.; Coronado, E.; Gaita-Ariño, A.; Palii, A. SIMPRE: A Software Package to Calculate Crystal Field Parameters, Energy Levels, and Magnetic Properties on Mononuclear Lanthanoid Complexes Based on Charge Distributions. *J. Comput. Chem.* **2013**, *34* (22), 1961–1967.

(14) Chilton, N. F.; Collison, D.; McInnes, E. J. L.; Winpenny, R. E. P.; Soncini, A. An Electrostatic Model for the Determination of Magnetic Anisotropy in Dysprosium Complexes. *Nat. Commun.* **2013**, *4*, 2551.

(15) Baldoví, J. J.; Borrás-Almenar, J. J.; Clemente-Juan, J. M.; Coronado, E.; Gaita-Ariño, A. Modeling the Properties of Lanthanoid Single-Ion Magnets Using an Effective Point-Charge Approach. *Dalton Trans. Camb. Engl. 2003* **2012**, *41* (44), 13705–13710.

(16) Baldoví, J. J.; Clemente-Juan, J. M.; Coronado, E.; Duan, Y.; Gaita-Ariño, A.; Giménez-Saiz, C. Construction of a General Library for the Rational Design of Nanomagnets and Spin Qubits Based on Mononuclear F-Block Complexes. The Polyoxometalate Case. *Inorg. Chem.* **2014**, *53* (18), 9976–9980.

(17) Monteiro, B.; Coutinho, J. T.; Pereira, C. C. L.; Pereira, L. C. J.; Marçalo, J.; Almeida, M.; Baldoví, J. J.; Coronado, E.; Gaita-Ariño, A. Magnetic Properties of the Layered Lanthanide Hydroxide Series YxDy8-x(OH)20Cl4·6H2O: From Single Ion Magnets to 2D and 3D Interaction Effects. *Inorg. Chem.* **2015**, *54* (4), 1949–1957.

(18) J. Baldoví, J.; Gaita-Ariño, A.; Coronado, E. Modeling the Magnetic Properties of Lanthanide Complexes: Relationship of the REC Parameters with Pauling Electronegativity and Coordination Number. *Dalton Trans.* **2015**, *44* (28), 12535–12538.

(19) Baldoví, J. J.; Duan, Y.; Morales, R.; Gaita-Ariño, A.; Ruiz, E.; Coronado, E. Rational Design of Lanthanoid Single-Ion Magnets: Predictive Power of the Theoretical Models. *Chem. – Eur. J.* **2016**, *22* (38), 13532–13539.

(20) Escalera-Moreno, L.; Suaud, N.; Gaita-Ariño, A.; Coronado, E. Determining Key Local Vibrations in the Relaxation of Molecular Spin Qubits and Single-Molecule Magnets. *J. Phys. Chem. Lett.* **2017**, *8* (7), 1695–1700.